Applied Thermal Engineering 62 (2014) 113–122

Contents lists available at ScienceDirect

Applied Thermal Engineering

journal homepage: www.elsevier.com/locate/apthermeng

Thermal management of a multiple mini-channel heat sink by the integration of a thermal responsive shape memory material

E. Di Maio [a], R. Mastrullo [b], A.W. Mauro [b,*], D. Toto [b]

[a] Department of Chemical, Materials and Production Engineering, Faculty of Engineering, University of Naples Federico II, P.le Tecchio 80, 80125 Naples, Italy
[b] Department of Industrial Engineering, University of Naples Federico II, P.le Tecchio 80, 80125 Naples, Italy

HIGHLIGHTS

- A novel application of a SMP material is investigated for the thermal management of a heat sink.
- Numerical simulations to find the matching of the heat sink and material system after regulation were carried out.
- The investigated system is able to control the heat sink temperature.
- Further analysis for system stability are required.

ARTICLE INFO

Article history:
Received 22 May 2012
Accepted 28 August 2013
Available online 14 September 2013

Keywords:
Shape memory polymers
Adaptive fluid control
Mini channel heat sink
Thermal management
Micro-valves

ABSTRACT

In this paper, a novel application of a thermo-responsive shape memory polymer (SMP) is proposed to smart-control the forced flow of water in a multi mini-channel heat sink. In particular, it is reported that millimeter-sized cylinders made of SMP could be used to smartly obstruct the fluid flow by adapting the flow cross section to the heat load to be removed. By integrating the sensing, the control and the actuation functions within a unique, millimeter-sized device, these micro-valves, unlike the traditional actuators normally used for flow control, could be easily embedded into small heat sinks, with significant space and energy saving, useful, in particular, in systems where several miniaturized components have to be cooled concurrently, such as the modern mainframes or the concentrated photovoltaic solar cells.

Two possible configurations for the SMP were considered in this study: an “open” configuration, without any obstruction of the water flow free and an “obstructed” configuration, with the millimeter-sized cylinder partially occupying the mini-channel. A numerical, steady state analysis was carried out with water in single-phase forced convection, to determine the effect of these two states on the internal fluid flow characteristics under different conditions of heat flux and pressure drop and to evaluate the overall thermal behavior of the smart-controlled multiple mini-channel heat sink in terms of ability to control the temperature of the system and to reduce the energy consumption.

1. Introduction

Thermal management of systems is a multi-objective engineering optimization problem, involving several design aspects of heat transfer (fluid circuitry, shape and size of the heat exchanger, material) and control (strategies and techniques, measurement devices, actuators). Each of these aspects can be more relevant than others depending on the specific field of application.

In the last decade, two important applications involved the design of compact heat exchangers: high computing power datacenters and concentrated photovoltaic systems. In these applications, it is know that fluxes as high as 400 MW/m^2 could be reached and that the passive cooling systems with natural air or forced air systems have reached their physical limits and are not cost effective [1].

Solutions with high thermal capacity fluids (single-phase forced water or two-phase flows) have been introduced, mainly focusing on heat transfer and pressure drops characteristics, in different fluid circuitry [2–13].

Actually, emerging miniaturized systems for heat sinks require complex architectures in which several concurrent flows occur, while a unique cooling system is available. Even if the use of two-phase flow is the best solution for stable temperature control in highly variable heat load systems, pressure drops, flow instabilities

* Corresponding author. Tel.: +39 081 7682198; fax: +39 081 2390364.
E-mail address: wmauro@unina.it (A.W. Mauro).

1359-4311/$ – see front matter © 2013 Elsevier Ltd. All rights reserved.
http://dx.doi.org/10.1016/j.applthermaleng.2013.08.039

and environmental impact of the refrigerants have to be taken into account, while water represents an environmental safe option (in single-phase forced convection).

Concerning the control of the system, the distribution of the coolant through concurrent pipelines by valves, temperature sensors and controllers for each flow line is not a reliable option in complex and miniaturized geometries, where space saving is of primary importance and, therefore, new compact options have to be considered.

Recently, integrated micro-valves, automatic valves and pumps with multi-purpose functionalities are emerging for the efficient control of fluids, in both fluidic and microfluidic. Micro-valves, in particular, are miniaturized devices able to close or open a fluid flux within a miniaturized fluid circuit, for example in ink-jet printers and fuel injection, biotechnology, heat management and display technologies. A review on mechanisms and applications has been provided by Kwang and Ahn [14], which categorized micro-valves as active, using mechanical and non-mechanical moving parts, and passive. The non-mechanical, active ones are of particular interest in terms of simplicity of device structure, low energy consumption and possibility to integrate sensing, controlling and the actuating functions. Micro-valves, then, with these integrated functions, may be referred to, more generally, as "microfluidic flow controllers", with the relevant "smart" feature, allowing for a smart-control of fluids, paving the way to new devices and potential applications [15,16].

Typically, microfluidic flow controllers are achieved via a creative use of some special types of polymers, which, due to physical and/or chemical features, have stimuli-responsive or smart abilities to respond to slight changes in the surrounding environment (in terms of temperature, solvent composition, pH, salinity, electric fields, specific antigens, and light, to list a few) with a volume, shape, or surface characteristic change. In particular, the polymers adapting their shape to the environment are addressed to as Shape Memory Polymers (SMPs), which may be considered as dual-shape materials that can switch from a temporary shape to a permanent shape. The temporary shape is, e.g., obtained by mechanical deformation and subsequent fixation of that deformation, which is then lost, in favor of the permanent shape, after a proper stimulus is given to the material. From the pioneering work from Kuhn et al. on muscle-like working polymer network [17], a number of papers dealt with the use of polymers that respond to external stimuli. Reviews on the use of smart polymers as micro-valves have been presented by Moorthy and Beebe [18] and Roy and Gupta [19], while a materials point of view, with the description of possible physical forms of polymers capable of showing smart characteristics, has been provided by Kumar et al. [20].

This work proposes the use of a smart and embedded flow regulation system based on SMPs where the stimulus for the actuation (shape change of the SMP) is provided by an increase of temperature of the flowing water, through each and every channel of the heat sink, induced by an increase of heat load to be dissipated at a fixed mass flow rate. The shape change of the SMP, which occurs across the so-called "switch temperature", programmed a priori, could be exploited to obtain an increase of the coolant flow passage, by a decrease of the head loss, independently and automatically for each and every channel, depending on the fluid temperature and, in turn, on the heat load to be removed from the part of the device adjacent to that channel.

To better describe the principle of operation, it is possible to refer to the scheme reported in Fig. 1, where a typical single channel is depicted. At the exit of each channel, a layer of a SMP is deposited such to form a plate. At ambient temperature the plate has a projection (temporary shape), which penetrates the channel and reduces the flow passage in the position where the fluid temperature reaches its maximum (Fig. 1(a)). In the case of a local, large increase of the heat load, at constant mass flow rate, the coolant temperature increases, eventually exceeding the switch temperature of the polymer, thereby inducing the contraction of the polymer projection (Fig. 1(b) and (c)). The corresponding decrease of the head loss results in a rapid increase of the coolant flow rate and of the

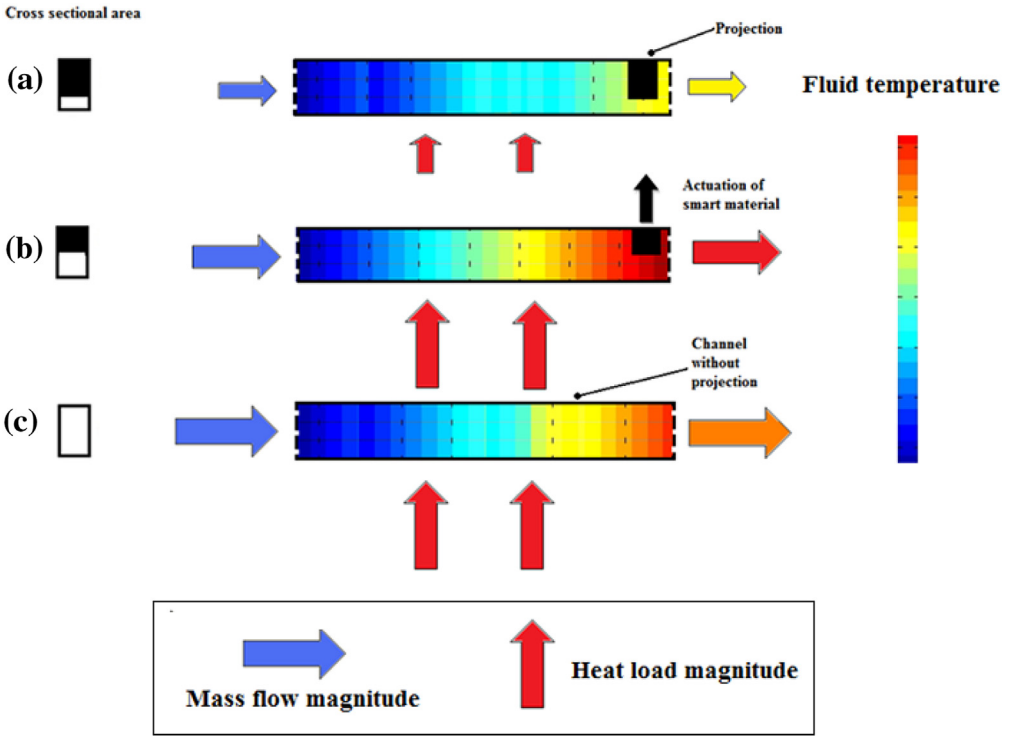

Fig. 1. Actuation of projection into the channel due to the change of the applied heat load.

removed heat and, in turn, in a decrease of the temperature of the device. Eventually, when the heat load decreases, the fluid temperature drops below the switch temperature of the polymer, and the SMP returns to its temporary shape.

The aim of this study is to numerically verify this concept to a multi mini-channel geometry. The internal fluid flow characteristics of the system in both the free and the partially-obstructed configuration was evaluated by means of numerical, steady state simulations with forced water under varied conditions in terms of heat flux and pressure drop. Furthermore, the system (heat sink and SMP) was coupled to a pumping system to evaluate its behavior in terms of ability to control the temperature of the system and, eventually, reduce the energy consumption.

2. Description of the computational domain and the mathematic model

In this section, the geometry of the water cooled multi mini channel sink and of the shape memory polymer plate (in the flat and "with protrusion" configurations), and the thermo-physical properties of the materials are described, together with the main governing equations of the model and the boundary conditions.

2.1. Description of the geometry and the thermo-physical properties: heat sink and SMP plate

Fig. 2(a) shows a 3D view of the multi mini-channel heat sink considered in this study. It is made of aluminum, with a thermal conductivity (k_{Al}) equal to 204 W/mK, and is composed of seven (N_{ch}) channels, each 3 mm in height (H_{ch}) and 2 mm wide (W_{ch}), with a 1.85 mm wall thickness (W_f). The mini-channels are 35 mm long in the flow direction (L_{ch}). The distance between the channels base and the heat sink base is 4.5 mm (t). Two plenums are disposed symmetrically at the entrance and at the exit of the channels. On the rear face of the heat sink, a square housing is designed to guide the positioning of the device to be cooled. This housing defines the heat transfer area (A_b) equal to 6.50 cm^2. Fig. 3 shows the technical drawing of the heat sink.

The "smart" part of the device is a SMP, flat plate (permanent shape) where, by compression molding, a temporary shape is produced having on one side seven (N_{ch}) cylindrical projection which, when mounted in the heat sink, partially obstruct the end of each channel, as shown in Fig. 2(b). The projections are 2.00 mm wide (W_p), 2.00 mm long (L_p) in the flow direction and 2.30 mm high (H_p), returning a 77% (H_p/H_{ch}) reduction of the cross sectional area of the channels. In this exemplificative study, the polymer belongs to the class of Shape Memory Polyurethanes (SMPU) [15,16], a novel class of functional materials, which has been extensively studied since their discovery in 1988 and attracting a great deal of attention due to their unique properties such as the wide range of shape recovery temperatures (from −30–70 °C), high shape recoverability and good processability. In comparison to metallic shape-memory alloys, the cycle of programming and recovery can take place in a much shorter time interval and polymers allow for a much higher deformation rate between shapes. This polymer is a linear or a lightly cross-linked copolymer, in which one segment may act as a switching segment and switching occurs at the glass transition temperature or at the melting temperature of that segment [17]. In effect, SMPUs allow for a fine tuning of the switch temperature to the specific application, by simply selecting the proper polymer segment within the copolymer.

2.2. Governing equations of the flow

The commercial CFD code Fluent was used to carry out the numerical simulations. The RNG K-model was considered for this purpose.

The set of governing equations used, for the steady state, neglecting the buoyancy, are listed below:

Continuity equation:

$$\frac{\partial}{\partial x_i}(\rho\langle u_i\rangle) = 0 \tag{1}$$

Momentum equation:

$$\rho\langle u_j\rangle\frac{\partial\langle u_i\rangle}{\partial x_j} = -\frac{\partial\langle p\rangle}{\partial x_i} + \frac{\partial}{\partial x_j}\left[(\mu+\mu_t)\left(\frac{\partial\langle u_i\rangle}{\partial x_j}+\frac{\partial\langle u_j\rangle}{\partial x_i}\right)\right] \tag{2}$$

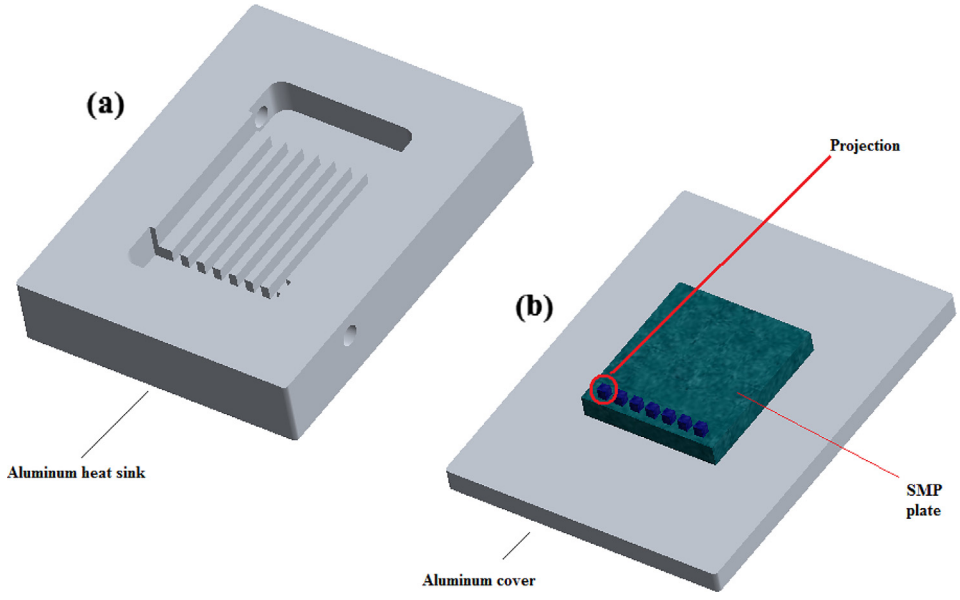

Fig. 2. 3D views: multi mini cannel heat sink (a), SMP plate (b).

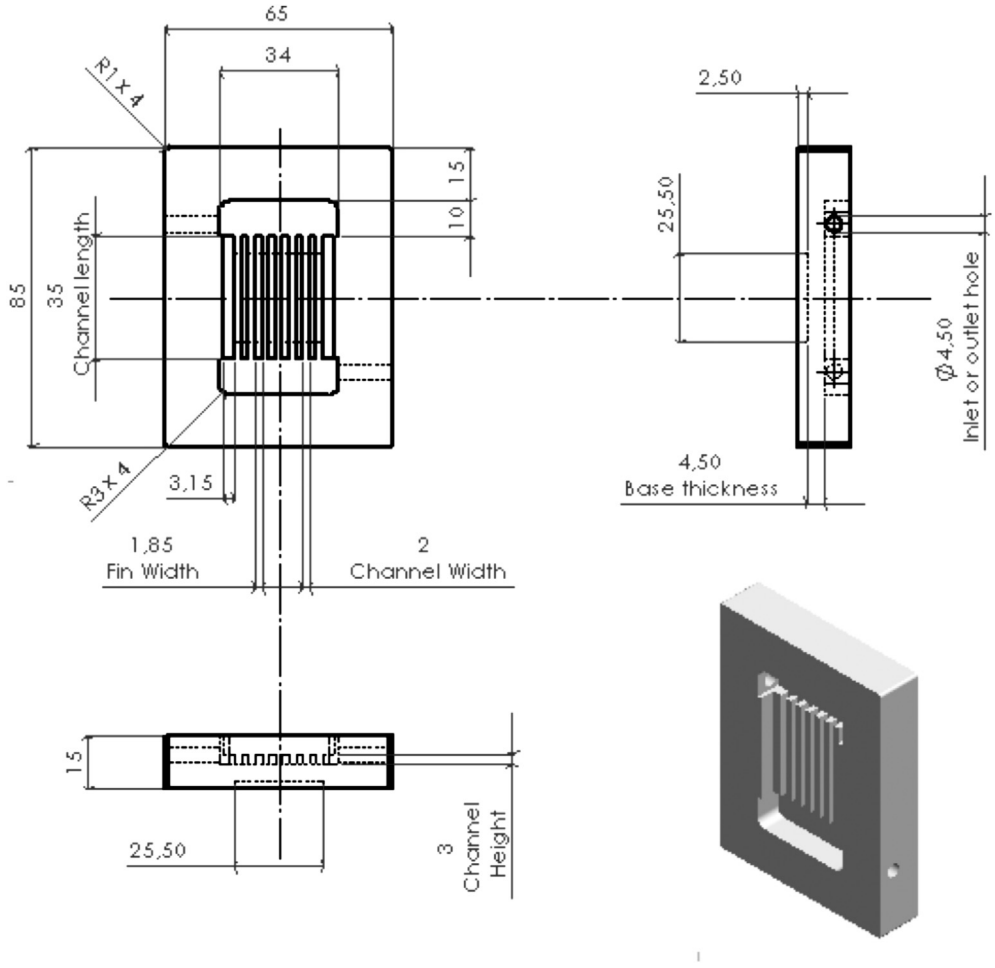

Fig. 3. Technical drawing of the multi mini channel heat sink (units: mm).

Energy equation:

$$\rho\langle u_j\rangle c_p\frac{\partial\langle T\rangle}{\partial x_j} = \frac{\partial}{\partial x_j}\left[(k+k_t)\frac{\partial\langle T\rangle}{\partial x_j}\right] \tag{3}$$

Turbulent kinetic energy (K) equation:

$$\frac{\partial}{\partial x_i}(\rho\langle u_i\rangle K) = \frac{\partial}{\partial x_i}\left[\frac{\mu_t}{\sigma_K}\frac{\partial K}{\partial x_i}\right] + P_k - \rho\varepsilon \tag{4}$$

Turbulent kinetic energy dissipation (ε) equation:

$$\frac{\partial}{\partial x_i}(\rho\langle u_i\rangle \varepsilon) = \frac{\partial}{\partial x_i}\left[\frac{\mu_t}{\sigma_\varepsilon}\frac{\partial \varepsilon}{\partial x_i}\right] + C_1\frac{\varepsilon}{K}P_k - C_2\rho\frac{\varepsilon^2}{K} \tag{5}$$

where μ_t is the eddy viscosity (in Eqs. (2), (4) and (5)) while k_t is the eddy thermal conductivity (in Eq. (3)) and can be calculated as follows:

$$\mu_t = C_\mu\rho\frac{K^2}{\varepsilon} \tag{6}$$

and

$$k_t = \frac{c_p\mu_t}{\sigma_t} \tag{7}$$

where C_μ is a constant equal to 0.085, ρ is the water density, c_p is the water specific heat and σ_t is the turbulent Prandtl number set equal to 1.0. Furthermore, the constants σ_K and σ_ε, respectively, in Eqs. (4) and (5) are both equal to 0.7179, the constant C_2 in Eq. (5) is equal to 1.68, whereas the term P_k in Eqs. (4) and (5) represents the production of turbulent kinetic energy.

Unlike the standard $K-\varepsilon$ model, in the RNG model the parameter C_1 is dependent on K and ε as follows:

$$C_1 = C_0 - \frac{\eta\left(1-\frac{\eta}{\eta_0}\right)}{1+\beta\eta^3} \tag{8}$$

where η is defined as:

$$\eta = \frac{K}{\varepsilon}\sqrt{\frac{P_k}{\mu_t}} \tag{9}$$

Finally, the non-dimensional constants η_0, C_0 and β are equal, respectively, to 4.38, 1.42 and 0.015.

Pressure boundary conditions were applied at the inlet and outlet of the heat sink and constant heat flux boundary condition was applied at the base of the heat sink. The water inlet temperature was kept constant. The remaining surfaces were set adiabatic.

The numerical computation was carried out with a finite volumes approach, by using the implicit method and the segregated solver. The simulations were stopped when the square root of the

Table 1
Test conditions.

Geometric configurations		
r	0; 0.77	
Boundary conditions		
T_{in}	27	°C
Δp	125; 500; 1000; 2000	Pa
q_b	25; 50; 75; 100	W/cm^2

sum of the squares of the individual outgoing residuals over all the computational nodes satisfied the criterion of 10^{-6} for the velocity components and 10^{-8} for the temperature and the pressure.

3. Results and discussion

Table 1 reports the conditions for the numerical tests conducted in this study. In details, the simulations were carried out by changing the reduction ratio $r = H_p/H_{ch}$. At H_{ch} equal to 2.3 mm, $r = 0.77$ (the cross sectional area is reduced near the exit by 77%), this value corresponding to the heat sink configuration with the SMP in its temporary shape (before actuation). At $r = 0$, the channels have no projections; this value corresponds to heat sink after the actuation of the SMP (permanent shape). Each geometry was tested at different base heat flux, q_b, from 0 to 100 W/cm^2 and the water pressure drop between the inlet and the outlet, Δp, from 125 to 2000 Pa. For each test, the inlet water temperature, T_{in}, was set equal to 27 °C. The imposed base heat flux, the pressure at inlet and the outlet and the water inlet temperature are part of the boundary conditions introduced in the Section 2.2.

3.1. Preliminary tests

Before carrying out the numerical campaign, the grid dependence of the solution was assessed. Each grid is formed by tetrahedral elements at variable density, in order to take into account the geometric curvatures and the fluid gradients. Several sizes of the grids were considered for this analysis. Table 2 reports the results for the three tested grids with a different number of cells, namely, 10^5, 4×10^5, 5×10^5 cells, to show the variations in results depending on the grid size, for the heat sink having no projections ($r = 0$). In particular, the water outlet temperature, T_{out}, the water mass flow rate, m, and the mean base temperature of the heat sink, $T_{b,m}$, are reported at constant heat flux and water pressure drop. The mean base temperature is computed at the heat transfer area, A_b. It is worth noting that, for this study, the aforementioned parameters are the main parameters suitable to drive conclusions about the general performance of the system and to evaluate the effects of the introduction of a SMP in the multi mini-channel heat sink. It can be noted, furthermore, that the grid with the 4×10^5 elements provides a satisfactory solution due to the negligible variation of the aforementioned quantities with respect to the 5×10^5 cells grid.

Table 2
Grid independence test.

$r = 0$ $T_{in} = 27$ °C $\Delta p = 2000$ Pa $q_b = 25$ W/cm^2		G3	G2	G1
Number of cells		5×10^5	4×10^5	1×10^5
m	(g/s)	19.28	19.30	19.76
Δm	(%)	–	0.10	2.49
T_{out}	(°C)	29.09	29.10	29.05
ΔT_{out}	(%)	–	0.03	−0.14
$T_{b,m}$	(°C)	34.09	33.75	33.3
$\Delta T_{b,m}$	(%)	–	−1.00	−2.32

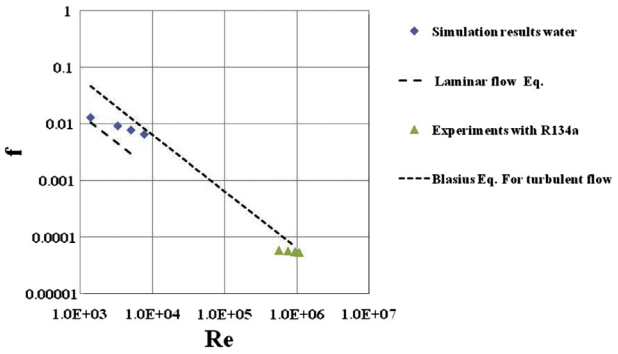

Fig. 4. Comparison of the Fanning factor, f, vs. the Reynolds number, Re, based on numerical results, experiments and prediction methods.

In fact, as it may be expected, the selection of finer grid elements allows for a complete relaxation of the residuals in pressure and velocity distributions. However, minor effects on the quantities relevant to this study were observed and the value of 4×10^5 for the number of grid elements was selected for the following tests.

As a second step, the effect of temperature on the water viscosity was estimated. For this purpose, several simulations were made by allowing the water dynamic viscosity to change as function of temperature. The resulting variation of the mass flow rate was within 2% with respect to the case with constant viscosity, which has been considered negligible for our purposes. In the following, water dynamic viscosity was kept constant. Water properties used were: density (ρ) 998.2 kg/m^3; specific heat (c_p) 4182 J/kg K; thermal conductivity (k) 0.610 W/mK and dynamic viscosity (μ) 1.003 mPa s. The pressure at the inlet was supposed large enough to guarantee that the water is in liquid phase all along the channel.

3.2. Comparison of numerical results with experiments and correlations

To have a verification of the numerical results, an experimental campaign was conducted, by using the test facility and of the data reduction procedure reported in Ref. [13]. Here, we adapted the test section and ran the experiment in adiabatic conditions in single-phase flow with a refrigerant (R134a). In particular for laminar flows the Fanning factor, f, is considered as a function of the Reynolds number, Re. In this case the Poiseuille number (Fanning factor multiplied by Reynolds) is a constant, depending only on the aspect ratio according to Eq. (5) reported in Ref. [21]; while for turbulent flows the Blasius equation was used (also available in Eq. (6) reported in Ref. [21]), where f is inversely proportional to the Re.

Fig. 4 shows the results of the comparison among the theoretical, numerical and the experimental results. In particular, it is possible to observe that the numerical results of the model stand in a range of Reynolds numbers across the transition from laminar to turbulent flows (the transition number estimated is around 2200 for this geometry; some speculation about that is available in Morini [22]). The numerical results lie between the equations for laminar and turbulent flows as expected. Moreover, to verify the validity of the Blasius equation for the experimental set-up, the experiments with R134a in single-phase are used, with a very good agreement.

About the energy equation this comparison is not presented: in fact, once mass flow rate input was checked for the fixed boundary conditions according to the previous analysis, this comparison should be an identity, since the model for the thermo-physical properties calculations is the same both for the experimental data reduction and for the numerical simulations. In this case the agreement among the results is more related to the validity of the

adiabatic assumption for the experiments than to the validation of the model itself. It is worth noting that this conclusion is correct, since the energy equation is independent on the continuity and momentum equation being the variation of the thermo-physical properties with temperature neglected.

3.3. Velocity, pressure and temperature distributions: the effect of the actuation

In this section, the velocity, the pressure and the temperature distributions are reported to give a more comprehensive understanding of the effects of the SMP actuations and, in particular, to show the effect of the boundary conditions on the temperature distribution of the rear face of the heat sink and the water velocity distribution. To this purpose, the geometrical configurations "with" and "without" the projections were considered ($r = 0.77$ and $r = 0$, respectively).

The water velocity distribution is computed on a plane parallel to the base of the heat sink at halfway of the channels. Since this plane intercepts the projections, the water velocity is zero in those zones, in the case $r = 0.77$. Fig. 5(a) shows, for the case $r = 0.77$, the increase of the water velocity when the water pressure drop is increased from 125 to 2000 Pa. Fig. 5(b) reports the temperature distribution in the same plane at constant base heat flux when the water pressure drop is increased from 125 to 2000 Pa. As expected, due to the better heat transfer, the temperature of the solid decreases with the increase of the water velocity. In the figure it is also shown the position of the heat exchanging channels, to evidence the shift toward the outlet of the hottest zone, consistently with the water flow direction.

Fig. 6 shows, in the same configuration ($r = 0.77$), the effect of the base heat flux on the temperature distribution on a plane parallel to the base of the heat sink at halfway of the channels. As it can be observed, at a pressure drop of 125 Pa, the temperature increases significantly when the base heat flux is increased from 25 to 100 W/cm^2.

Fig. 7 depicts the effect of the SMP actuation. After the actuation of the SMP ($r = 0$), as expected, the water velocity increased at fixed pressure drop, as clearly shown in Fig. 7(a) reporting a direct comparison of the two configurations, at pressure drop of 500 Pa. Of course, this effect is due to the removal of the projections, which impose, locally, a huge energy loss for the flow stream.

3.4. Global performance evaluation: temperature controlling and energy saving

After the validation of the model and the analysis of the effects of the boundary conditions on the velocity and temperature distributions, a more comprehensive performance analysis of the SMP integration as a control element is presented.

Table 3 shows the whole set of tested conditions and the numerical results. The simulations were carried out by taking into account two main parameters for each geometrical configuration: the volumetric flow rate V, to build the characteristic of the heat

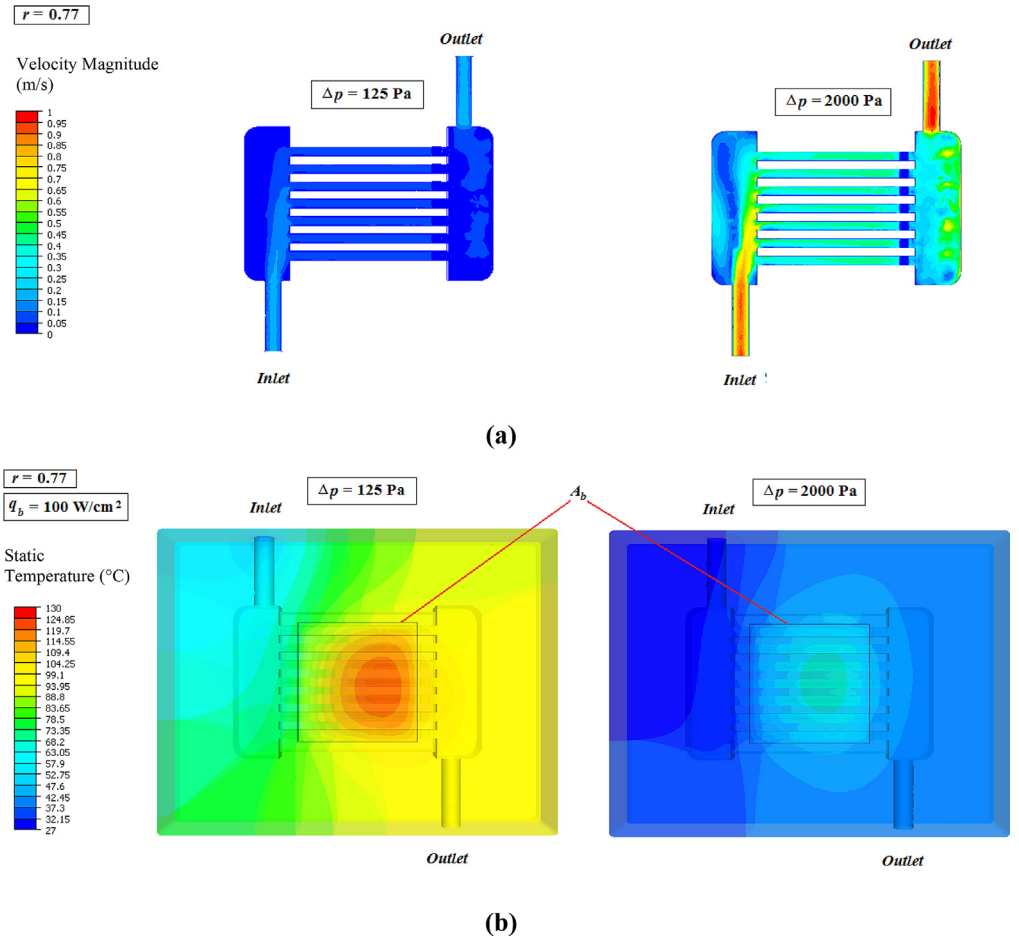

Fig. 5. Effect of a water pressure drop variation from 125 to 2000 Pa: (a) water velocity distribution and (b) temperature distribution, on a plane parallel to the base of the heat sink at halfway of the channels, for a constant base heat flux equal to 100 kW/cm^2 and $r = 0.77$.

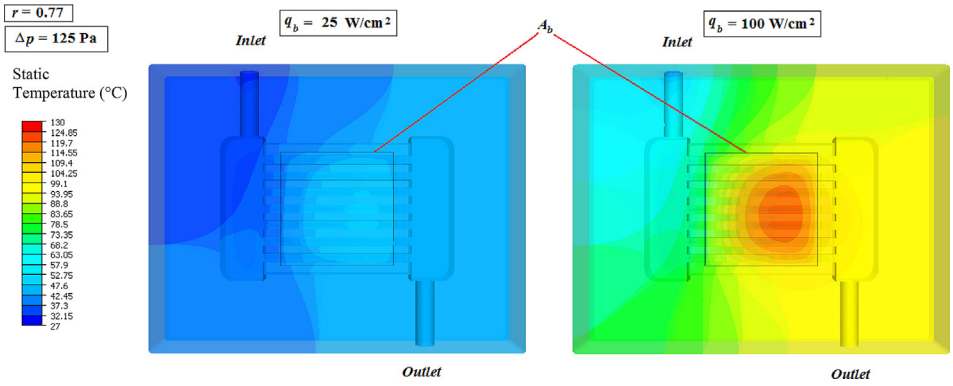

Fig. 6. Effect of a base heat flux variation from 25 to 100 kW/cm^2 on the temperature distribution computed on a plane parallel to the base of the heat sink at halfway of the channels, for a pressure drop equal to 125 Pa and $r = 0.77$.

sink and the maximum base temperature $T_{b,max}$, computed on the heat transfer area A_b, to evaluate the efficiency of the heat transfer. Also, the mean temperature of the projections of the SMP plate, T_p, was evaluated in order to estimate at which switch temperature T_{switch}, the SMP should to be "programmed" to undergo actuation. As it can be noted, values of V at fixed ΔP and r do not depend on temperature, since, as commented in Section 3.1, the water viscosity is set constant.

Fig. 8 shows the internal characteristic of the heat sink before and after the actuation of the SMP. At the same pressure drop, the water flowing through the heat sink before actuation ($r = 0.77$) resulted lower than the case corresponding to the heat sink after the actuation ($r = 0$). Moreover, this difference increased with the increase of the pressure drop. To estimate the variation of the water volumetric flow rate corresponding to the actuation, it is necessary to match the pump performance curve with the characteristic of

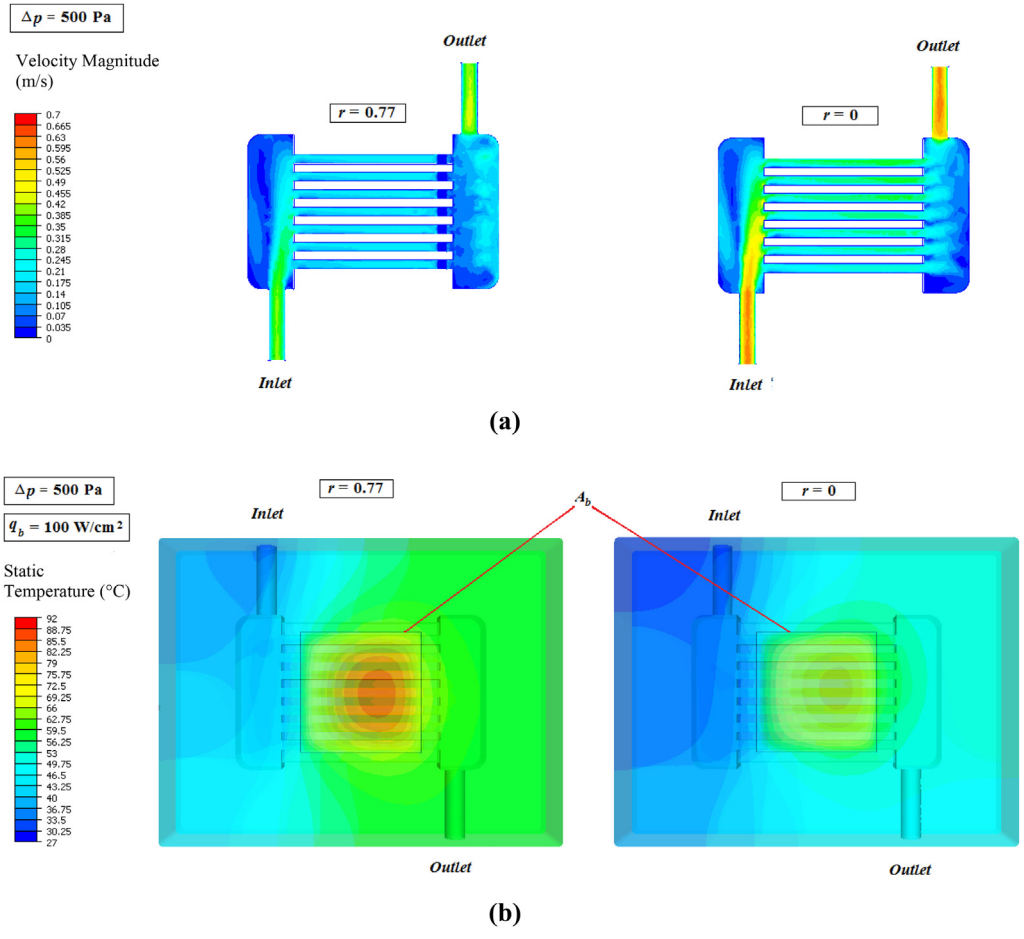

Fig. 7. Effect of the actuation of the SMP: (a) water velocity distribution and (b) solid temperature distribution, computed on a plane parallel to the base of the heat sink at halfway of the channels, for a pressure drop equal to 500 Pa and a base heat flux equal to 100 kW/cm^2.

Table 3
Numerical results.

Δp [Pa]	q_b [W/cm^2]	r [−]	V [l/h]	$T_{b,max}$ [°C]	$T_{b,m}$ [°C]	T_p [°C]	T_{out} [°C]	m [g/s]	$\varphi_b = (T_{b,max} - T_{in})/q_b$ [cm^{2}K/W]	$\varphi_p = (T_p - T_{in})/q_b$ [cm^{2}K/W]
125	25	0.77	7.86	52.4	47.8	43.5	43.9	2.18	1.02	0.66
		0	12.4	47.2	42.7	37.2	38.2	3.43	0.81	0.41
	50	0.77	7.86	77.9	68.6	60.1	60.9	2.18	1.02	0.66
		0	12.4	67.4	58.5	47.4	49.4	3.43	0.81	0.41
	75	0.77	7.86	103	89.3	76.6	77.8	2.18	1.02	0.66
		0	12.4	87.7	74.2	57.6	60.6	3.43	0.81	0.41
	100	0.77	7.86	129	110	93.2	94.7	2.18	1.02	0.66
		0	12.4	108	90.0	67.8	71.8	3.43	0.81	0.41
500	25	0.77	18.8	42.9	39.1	34.0	34.5	5.22	0.64	0.28
		0	29.4	40.3	36.7	31.5	31.9	8.16	0.53	0.18
	50	0.77	18.8	58.9	51.2	41.1	42.0	5.22	0.64	0.28
		0	29.4	53.7	46.5	36.0	36.7	8.16	0.53	0.18
	75	0.77	18.8	74.8	63.3	48.1	49.5	5.22	0.64	0.28
		0	29.4	67.0	56.2	40.5	41.6	8.16	0.53	0.18
	100	0.77	18.8	90.7	75.4	55.2	57.0	5.22	0.64	0.28
		0	29.4	80.3	66.0	45.0	46.5	8.16	0.53	0.18
1000	25	0.77	28.8	40.1	36.6	31.6	31.9	8.00	0.52	0.18
		0	45.2	38.1	34.9	30.0	30.2	12.5	0.44	0.12
	50	0.77	28.8	53.2	46.2	36.2	36.9	8.00	0.52	0.18
		0	45.2	49.2	42.9	33.0	33.4	12.5	0.44	0.12
	75	0.77	28.8	66.3	55.8	40.9	41.8	8.00	0.52	0.18
		0	45.2	60.4	50.8	36.1	36.6	12.5	0.44	0.12
	100	0.77	28.8	79.3	65.4	45.5	46.8	8.00	0.52	0.18
		0	45.2	71.5	58.8	39.2	39.8	12.5	0.44	0.12
2000	25	0.77	44.8	37.9	34.8	30.0	30.2	12.4	0.44	0.12
		0	69.6	36.6	33.8	29.0	29.1	19.3	0.38	0.081
	50	0.77	44.8	48.8	42.6	32.9	33.4	12.4	0.44	0.12
		0	69.6	46.2	40.5	31.0	31.2	19.3	0.38	0.081
	75	0.77	44.8	59.8	50.4	35.9	36.6	12.4	0.44	0.12
		0	69.6	55.8	47.3	33.1	33.3	19.3	0.38	0.081
	100	0.77	44.8	70.7	58.1	38.9	39.8	12.4	0.44	0.12
		0	69.6	65.4	54.0	35.1	35.4	19.3	0.38	0.081

the heat sink, as reported in the same Fig. 8, where it is proved that V increases by more than 50% when r decreases from 0.77 to 0.

In order to assess the possible increase in the thermal performance after the actuation of the SMP a parameter was defined as follow:

$$\varphi_b = \frac{T_{b,max} - T_{in}}{q_b} \tag{10}$$

This term has the same dimensions of a thermal resistance per unit of area (cm^{2}K/W) and relates the maximum base temperature to the thermal boundary conditions (temperature of the fluid at the inlet and base heat flux).

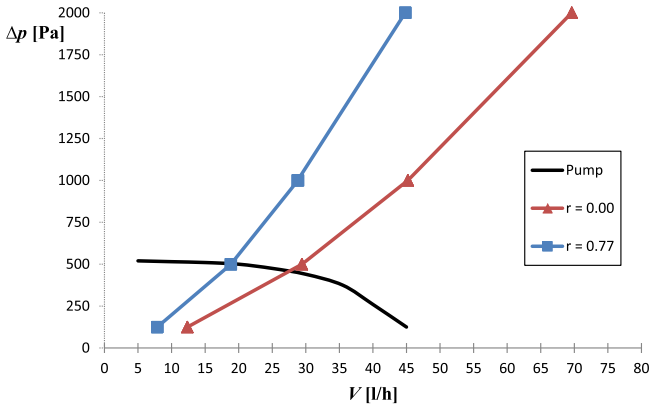

Fig. 8. Matching between the pump performance curve and the characteristic of the heat sink before and after the actuation of the SMP.

Assuming a 1-D variation of the fluid temperature along the channel, in a single-phase flow it reaches the maximum temperature at the exit.

From the energy balance between the inlet and the outlet of the multi mini channels system (in steady state conditions, neglecting heat losses), it follows:

$$q_b A_b = \rho V c_p (T_{out} - T_{in}) \tag{11}$$

At the same time, assuming steady state 1-D heat flux along the direction perpendicular to the base, the difference between the maximum base temperature and the outlet water temperature, T_{out}, can be written as the overall thermal resistance, R, which is the sum of the conductive and the convective thermal resistances:

$$\frac{(T_{b,max} - T_{out})}{q_b} = \left(\frac{t}{k_{Al}} + \frac{A_b}{h_m N_{ch} \left(W_{ch} + 2\eta_{fin} H_{ch} \right) L_{ch}} \right) \tag{12}$$

where η_{fin} is the fin efficiency and h_m is the area averaged convective heat transfer coefficient, that depends mainly on the volumetric flow rate.

By solving Eq. (11) respect to T_{out} and combining it with Eq. (12), it is possible to re-arrange the definition as by Eq. (10):

$$\varphi_b = \frac{T_{b,max} - T_{in}}{q_b} = \left(\frac{t}{k_{Al}} + \frac{A_b}{h_m N_{ch} \left(W_{ch} + 2\eta_{fin} H_{ch} \right) L_{ch}} + \frac{A_b}{\rho c_p V} \right) \tag{13}$$

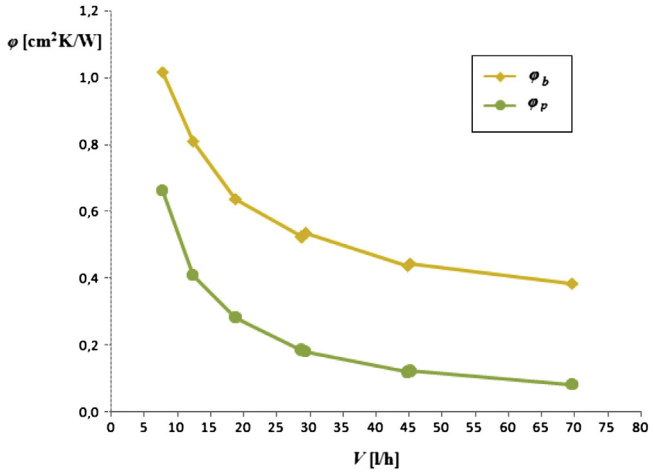

Fig. 9. φ_b and φ_p vs. water volumetric flow rate.

It can be noted that, at constant volumetric flow rate, all of the terms in the r.h.s. of Eq. (13) are constant, and, as a consequence, φ_b is also constant. This result is confirmed by the numeric simulations both at $r = 0.77$ and at $r = 0$, as shown in Table 3.

In the same way, it is possible to define a ratio of the difference between the mean surface temperature of the projections and the water inlet temperature over the base heat flux, namely:

$$\varphi_p = \frac{T_p - T_{in}}{q_b} \cong \frac{T_{out} - T_{in}}{q_b} = \frac{A_b}{\rho c_p V} \tag{14}$$

which returns the difference between the averaged surface temperature of the projections and the water inlet temperature over the base heat flux. It has the same dimensions of φ_b and relates the actuation temperature of the SMP to the thermal boundary conditions. It can be useful to represent the whole process on the operating map depicted in Fig. 10, which groups the three plots together: on the upper right corner (I) and on the lower right corner (II) the plots of Figs. 8 and 9 are reported, respectively; on the lower left corner (III), different isothermal curves of the maximum base temperature (yellow line) and the mean temperature of the projections (green line), computed, respectively, as by Eqs. (12) and (13), are reported in a φ vs. q_b coordinate system at a water inlet temperature of 27 °C.

In a condition of low base heat flux, the projection of the SMP restricts the flow passage ($r = 0.77$) and the working condition is represented by point A in Fig. 10 (corner (I)). The corresponding V and φ_b values are represented by point B (corner (II)). It is then possible to know the heat flux, point D in corner (III), corresponding to a fixed maximum working temperature at the base (rear) of the heat sink equal to e.g. 75 °C (point C). Correspondingly, the actual working condition for φ_b is (point E) and the temperature of the projections is estimated by point F (48 °C).

Actually, if the switch temperature during the design was set to, for example, 48 °C (point F) and the base heat flux is less than $q_{C,D} = 75$ kW/cm^2, the projections close the passage of the fluid ($r = 0.77$). When the base heat flux overcomes $q_{C,D}$ at the same volumetric flow rate, the fluid temperature increases, and the temperature of the projection surface overcomes the switching temperature, opening the flow passage. Hence, the balancing point between the pump and the internal characteristic of the channels moves to point G in Fig. 10 (corner (I)). The system is able to work in a new condition where the new heat flux to reach at the same maximum temperature at the base is point K in Fig. 10 (corner (III)), corresponding to a value of 86 kW/cm^2.

In this way, the system is able to control the temperature under 75 °C with $r = 0.77$ for an heat flux up to 75 kW/cm^2 or switching between $r = 0$ and $r = 0.77$ for heat fluxes between 75 and 86 kW/cm^2, with the self-regulation of the projections.

Finally, in order to estimate the energy saving which could be obtained using this regulation system, the plots reported in Fig. 11

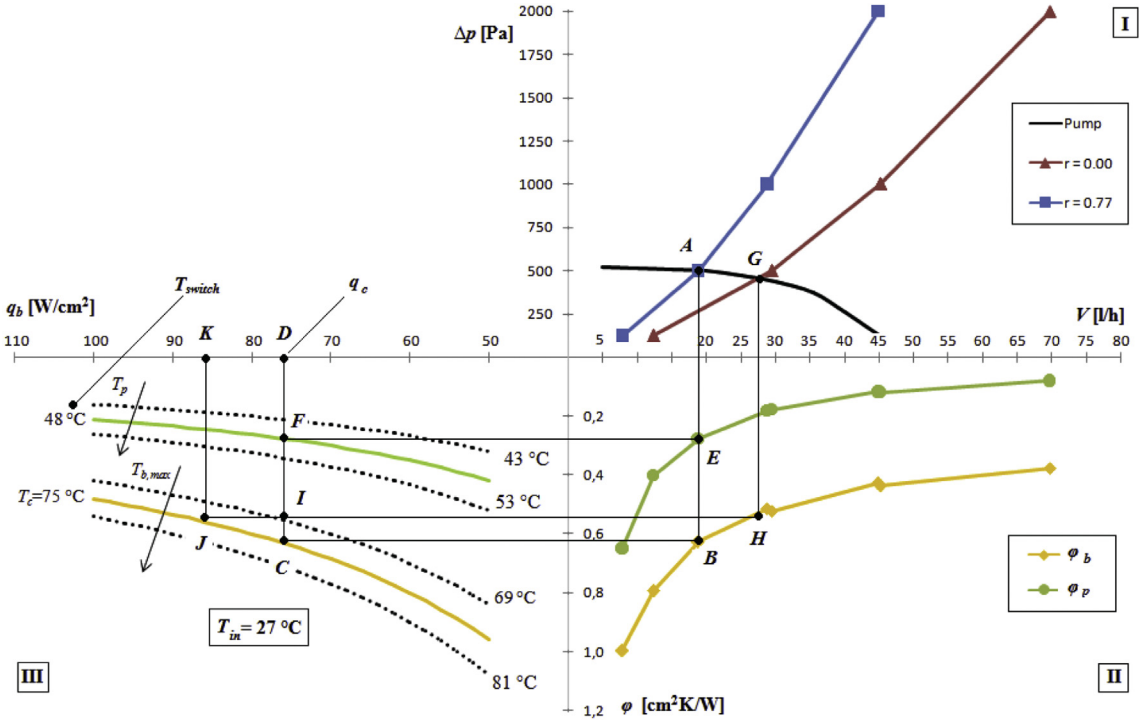

Fig. 10. Effect of the actuation of the SMP shown on the operating map at $T_{in} = 27$ °C: estimation of the switch temperature and the maximum base temperature variation.

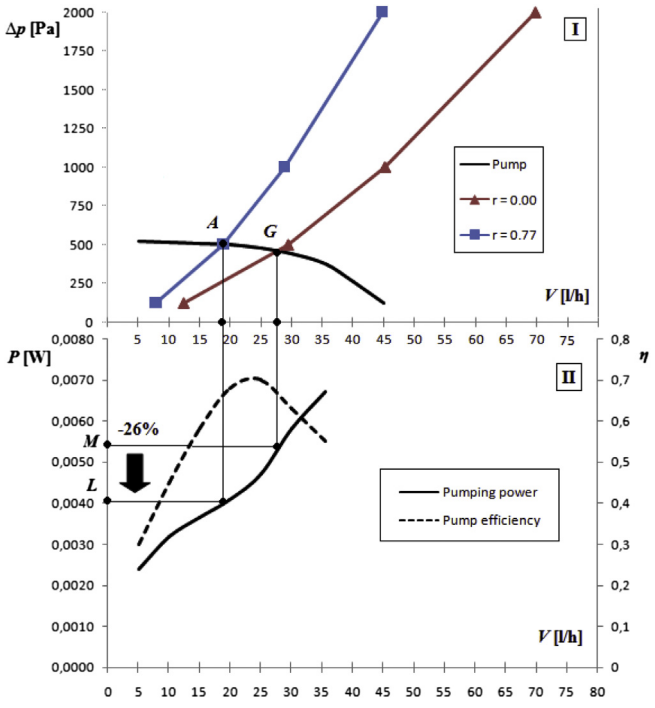

Fig. 11. Effect of the actuation of the SMP on the pumping power.

can be analyzed. Plot I shows the pump performance curve and the characteristic of the heat sink, while the plot II represents the pumping power as a function of *V*. Before the actuation, the volumetric flow, *V*, and the pumping power are obtained, respectively, by points A and L. Once the SMP is actuated ($r = 0$), *V* increases to point G, and, as a consequence, the pumping power increases to point M. Hence, whenever the base heat flux is less than the critical value $q_{c,D}$ which causes the actuation of the SMP, the pumping power is lower with respect to the maximum value. In this case, the pumping power is reduced by 26%.

Of course, the numerical results for temperatures and energy savings are strictly related to the configuration and operating conditions considered in this work; nevertheless the behavior of the system will be similar in any scaled system similar to this one (for example a different system could be designed to manage larger variations of the base heat flux).

4. Conclusions

This work introduced an integration of a Shape Memory Polymer (SMP) into a multiple mini channel heat sink to allow an automatic adaptation to heat flux variations. This solution could be interesting in complex miniaturized systems in which several concurrent flows have to be regulated depending on the local heat load, such as in the modern mainframes and concentrating photovoltaic solar panels. This particular kind of solution is potentially capable of regulating the flow passage of the channels sensing the variations of the fluid temperature, depending on the heat flux variations. A further advantage in using SMPs as smart flow regulators is that, unlike the traditional actuators, they could be easily embedded into small heat sinks, resulting in a significant space saving. As a result, they could be used to replace the traditional valves, the temperature sensors and the controllers usually used for the fluid flow regulation of heat sinks.

In order to investigate on this perspective, numerical calculations under steady state conditions were carried out on a system simulating a water cooled aluminum multi mini channel heat sink covered by an SMP plate with projections that partially obstruct the channels and reduce the cross sectional flow passage. Two geometric configurations, which represent the heat sink before and after the actuation of the SMP, were considered. The simulations were run by changing the imposed base heat flux and the water pressure drop between the inlet and the outlet of the heat sink.

First numerical results showed the potential advantages in using these materials to smartly regulate the coolant flow in a multi channel heat sink. At lower heat fluxes, the lower water flow rate which circulates through the heat sink because of the smaller cross sectional flow passage, limits the pumping power; while, at higher heat fluxes than a critical value, the increase of the water flow rate due to the actuation of SMP projections, allows to reduce the base temperature of the device to be cooled.

Since the simulations presented in this work were made under steady state conditions, no result about the time-response of the SMP plate during actuation is available. For this reason, a transient analysis is necessary to understand the operation of the system when periodic variations of the base heat flux are encountered or to explore unstable conditions.

References

[1] Assembly and Packaging, ITRS Roadmap, 2001, pp. 4–8.
[2] R. Chein, G. Huang, Thermoelectric cooler application in electronic cooling, Appl. Therm. Eng. 24 (2004) 2207–2217.
[3] H.Y. Zhang, D. Pinjala, T.N. Wong, K.C. Toh, Y.K. Joshi, Single-phase liquid cooled microchannel heat sink for electronic packages, Appl. Therm. Eng. 25 (2005) 1472–1487.
[4] H. Bhowmil, Convection heat transfer from discrete heat sourced in a liquid cooled rectangular channel, Appl. Therm. Eng. 25 (2005) 2532–2542.
[5] T. Bello-Ochende, L. Liebenberg, J.P. Meyer, Constructal cooling channels for micro-channel heat sinks, Int. J. Heat Mass Transfer 50 (2007) 4141–4150.
[6] P. Naphon, O. Khonseur, Study on the convective heat transfer and pressure drop in the micro-channel heat sink, Int. Commun. Heat Mass 36 (2009) 39–44.
[7] S.G. Kandlikar, Scale effects on flow boiling heat transfer in microchannels: a fundamental perspective, Int. J. Therm. Sci. 49 (2010) 1073–1085.
[8] P. Naphon, S. Klangchart, S. Wongwises, Numerical investigation on the heat transfer and flow in the mini-fin heat sink for CPU, Int. Commun. Heat Mass 36 (2009) 834–840.
[9] B. Agostini, J.R. Thome, M. Fabbri, B. Michel, High heat flux two-phase cooling in silicon multi-microchannels, IEEE Trans. Compon. Pack. T. 31 (2008) 691–701.
[10] B. Agostini, R. Revellin, J.R. Thome, M. Fabbri, B. Michel, D. Calmi, High heat flux flow boiling in silicon multi-microchannels: Part III – Saturated critical heat flux of R236fa and two-phase pressure drops, Int. J. Heat Mass Transfer 51 (2008) 5426–5442.
[11] J.E. Park, J.R. Thome, Critical heat flux in multi-microchannel copper elements with low pressure refrigerants, Int. J. Heat Mass Transfer 53 (2009) 110–122.
[12] A. Royne, C.J. Dey, D.R. Mills, Cooling of photovoltaic cells under concentrated illumination: a critical review, Sol. Energ. Mat. Sol. C. 86 (2005) 451–483.
[13] A.W. Mauro, J.R. Thome, D. Toto, G.P. Vanoli, Saturated critical heat flux in a multi-microchannel heat sink fed by a split flow system, Exp. Therm. Fluid Sci. 34 (2010) 81–92.
[14] W.O. Kwang, C.H. Ahn, A review of microvalves, J. Micromech. Microeng 16 (2006) R13–R39.
[15] A. Richter, G. Paschew, S. Klatt, J. Lienig, K.-F. Arndt, H.-J.P. Adler, Review on hydrogel-based pH sensors and microsensors, Sensors 8 (2008) 561–581.
[16] L. Dong, A.K. Agarwal, D.J. Beebe, H. Jiang, Adaptive liquid microlenses activated by stimuli-responsive hydrogels, Nature 442 (2006) 551–554.
[17] W. Kuhn, B. Hargitay, A. Katchalsky, H. Eisenberg, Reversible dilation and contraction by changing the state of ionization of high-polymer acid networks, Nature 165 (1950) 514–516.
[18] J. Moorthy, D.J. Beebe, Organic and biomimetic designs for microfluidic systems, Anal. Chem. 75 (2003) 292A–301A.
[19] I. Roy, M.N. Gupta, Smart polymeric materials: emerging biochemical applications, Chem. Biol. 10 (2003) 1161–1171.
[20] A. Kumar, A. Srivastava, I.Y. Galaev, B. Mattiasson, Smart polymers: physical forms and bioengineering applications, Prog. Polym. Sci. 32 (2007) 1205–1237.
[21] E.M. Steinke, S.G. Kandlikar, Single-phase liquid friction factors in microchannels, Int. J. Therm. Sci. 45 (2006) 1073–1083.
[22] G.L. Morini, Single-phase convective heat transfer in microchannels: a review of experimental results, Int. J. Therm. Sci. 43 (2004) 631–651.